PERGAMON

Carbon 39 (2001) 1075–1082

CARBON

Adsorption properties of nitrogen-alloyed activated carbon fiber

Cheol-Min Yang, Katsumi Kaneko*

Graduate School of Science and Technology, Chiba University, 1-33 Yayoi, Inage, Chiba 263-8522, Japan

Received 20 June 2000; accepted 29 August 2000

Abstract

N-alloyed activated carbon fibers (ACFs) were prepared by chemical vapor deposition (CVD) of pyridine on pitch-based ACF at 1023 K and 1273 K for 1 h. The N-alloyed ACFs were characterized by using the N_2 adsorption at 77 K, CO_2 adsorption at 273 K, elemental analysis, and X-ray photoelectron spectroscopy (XPS). The nitrogen content increases as a result of the pyridine-CVD. XPS examination showed that the percent of quaternary nitrogens in nitrogen structures increases remarkably from 60 to 91% for CVD temperatures of 1023 and 1273 K, respectively. The effects of N-alloying on adsorption properties of ACFs for C_2H_5OH and H_2O were examined at 303 K. Both N-alloyed ACFs have a larger fractional filling of C_2H_5OH molecules. The uptake pressure of the H_2O adsorption branches of both N-alloyed ACFs shifts to a lower relative pressure, compared with that of pristine ACF. Furthermore, the ratios of the V^{H_2O} (saturated amount of H_2O at $P/P_0 = 1$) to $W_0^{N_2}$ (pore volume determined by N_2 adsorption at 77 K) of N-alloyed ACFs are much larger than that of pristine ACF.

Keywords: A. Activated carbon; B. Chemical vapor deposition; C. Adsorption; D. Adsorption properties

1. Introduction

Activated carbon fibers (ACFs) have excellent adsorptivity due to large specific surface area, pore volume, and uniform microporosity. ACFs have been studied extensively both from fundamental and industrial aspects [1–3]. The adsorption properties of ACFs are controlled by their pore width and pore-wall chemistry. Hence the relationship between the pore width and adsorption characteristics has been actively studied [4–6]. As to the pore wall chemistry, the pore-walls of ACF are partially oxidized or modified with other chemical substances in order to get better adsorbents or catalysts [7–13]. In particular, the relationship between surface functional groups containing oxygen and adsorption properties for polar molecules has been widely studied [14–17]. However, the modification of the pore wall chemistry by alloying with foreign atoms such as nitrogen or boron atoms is not actively studied [18–21]. The porous carbon alloyed with nitrogen atoms should have a polar nature and vary its physical property. ACFs have slit-shaped micropores and nonpolar surfaces where nonpolar vapor molecules can be easily adsorbed even in a low pressure region. ACF of low amount of surface oxygen groups such as pitch-based ACF is not adequate for the adsorption of polar molecules such as water, alcohols etc. However, the fundamental reason why polar molecules are not adsorbed in hydrophobic carbon micropores is not obvious yet. If the pore-wall polarity can be controlled by alloying technique, the interaction of a polar molecule with the hydrophobic micropore should be better elucidated.

Kawabuchi et al. [19–21] modified ACF with chemical vapor deposition (CVD) of pyridine, inducing a high molecular sieving property. These authors applied their CVD method to get nitrogen-alloyed ACFs. In the preceding article [18], we reported the alloying procedures and the detailed characterization of nitrogen-alloyed ACFs. This paper describes the effect of nitrogen-alloyed micropore walls on the adsorption behavior for polar molecules.

2. Experimental

2.1. Preparation of nitrogen-alloyed ACFs

Pyridine was used for preparing N-alloyed ACFs (N-alloyed ACFs). Pitch-based ACF (A-20; Adohl Co.) was heated at 1273 K in argon before deposition of pyridine to

*Corresponding author. Tel.: +81-43-251-1111; fax: +81-43-290-2788.

E-mail address: kaneko@pchem2.s.chiba-u.ac.jp (K. Kaneko).

0008-6223/01/$ – see front matter
PII: S0008-6223(00)00229-3

remove oxygen surface groups. The deposition for 0.2 g of ACF was performed under the following conditions: flow rate of He carrier gas: 200 ml/min; time: 60 min, and temperature: 1023 and 1273 K. The ACF sample treated by the pyridine CVD at T K for t min is designated ACF/PyT-t in this paper. For example, ACF treated with pyridine at 1273 K for 60 min is described as ACF/Py1273-60.

2.2. Elemental analysis and X-ray photoelectron spectroscopy

Elemental analysis was performed using a Perkin-Elmer-2400 after pretreatment at 423 K for 2 h. X-ray photoelectron spectra were obtained using an ESCA-850 (Shimadzu). The measurements were performed with Mg K_α under a vacuum pressure $<10^{-6}$ Pa at room temperature. The acceleration tension and emission current of the nonmonochromatized X-ray source are 7 kV and 30 mA, respectively. The XPS spectra of all the samples were calibrated using the graphitic carbon C1s peak at 284.6 eV.

2.3. Adsorption of N_2 and CO_2

The micropore structures were determined by adsorption of N_2 at 77 K and CO_2 at 273 K using volumetric equipment (Quantachrome AS-1-MP) after preevacuation at 423 K and 10^{-4} Pa for 2 h. The micropore structural parameters were obtained from high-resolution α_s-plot and Dubinin–Radushkevich (DR)-plot.

2.4. Adsorption of C_2H_5OH and H_2O

The adsorption isotherms of C_2H_5OH and H_2O on the ACF samples were gravimetrically measured at 303 K. The sample was preevacuated at 10 mPa and 383 K for 2 h. C_2H_5OH and H_2O were purified by a repeated freeze-pump-thaw cycle before their introduction into the adsorption cell.

3. Results and discussion

3.1. Pore wall chemistry of N-alloyed ACFs

Table 1 shows the elemental composition of pristine and N-alloyed ACFs from the elemental analysis. The elemental analysis gives direct information on the average extent of nitrogen-alloying at the bulk state. Even the pristine ACF contains a small amount of nitrogen. The nitrogen content increases as a result of the pyridine-CVD. However, the nitrogen content decreases from 2.5 to 1.4 mol.% on raising the CVD temperature from 1023 to 1273 K. The surface chemical changes of ACFs after pyridine-CVD were examined by X-ray photoelectron spectroscopy (XPS). Since the surface nature is of great importance for the adsorption phenomena, it is worth studying the surface chemical changes of ACF after CVD. The data from the XPS analysis are also given in Table 1 for comparison to the bulk composition obtained by the elemental analysis. Table 1 shows the percent of nitrogen species determined from deconvolution of N1s XPS spectra by the Gaussian–Lorentzian mixed function (80–20%, respectively) [22,23]. The percent of quaternary nitrogens increases remarkably from 60 to 91% for CVD temperatures of 1023 and 1273 K, respectively. Fig. 1 shows the XPS spectral change of the C1s peak of pristine and N-alloyed ACFs. The C1s peak coincides with that of graphite (284.6 eV). The spectra clearly show a tendency of decrease of the C1s peak shoulder observed at the higher binding energy. This slight difference in the shoulder of intensity at the high

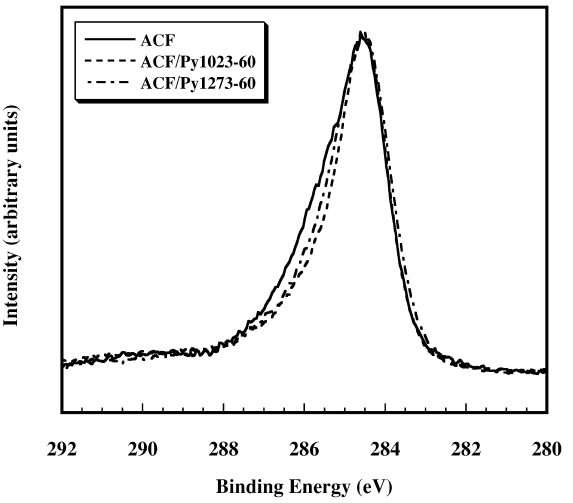

Fig. 1. C1s XPS spectra of pristine and N-alloyed ACFs.

Table 1
Chemical composition of pristine and N-alloyed ACFs from elemental analysis and XPS

Sample	Elemental analysis (mol.%)				XPS (%)	
	C	H	N	N/C	Pyridinic nitrogen	Quaternary nitrogen
ACF	93.6	2.4	0.3	0.004	–	–
ACF/Py1023-60	89.3	3.5	2.5	0.028	40	60
ACF/Py1273-60	92.2	1.2	1.4	0.015	9	91

binding energy side indicates the changes in the concentration of the surface functional groups. The typical oxygen-containing surface functional groups on the surface of the carbon materials are identified as representative phenolic or alcohol groups at 286.1 eV, carbonyl group at 287.6 eV, and carboxyl group at 288.6 eV [24–26]. A quantitative comparison of the high-energy region at the C1s spectra is desirable, but the differences are too small to evaluate the concentration of the surface functional groups. This decrease in intensity of high-energy side comes mostly from covering of the surface functional groups by deposited carbons. The surface functional groups are beneficial for adsorption of polar molecules due to dipole interactions, and thereby adsorption of polar molecules on the oxygen functional groups of N-alloyed ACFs should be smaller than that on pristine ACF.

3.2. N_2 and CO_2 adsorption of N-alloyed ACFs

Fig. 2 shows N_2 adsorption isotherms (77 K) of pristine ACF and N-alloyed ACFs treated at 1023 and 1273 K. All adsorption isotherms are of type I, suggesting the presence of uniform microporosity. The saturated amounts of N_2 adsorption at $P/P_0 = 1$ on ACF/Py1023-60 and ACF/Py1273-60 are 1.7 times smaller than that of pristine ACF. The CO_2 adsorption isotherms (273 K) at subatmospheric pressure on the samples are shown in Fig. 3. Both N-alloyed ACFs show a lower adsorption amount than that of pristine ACF. ACF/Py1023-60 has an enhanced adsorption compared with ACF/Py1273-60. However, we cannot obtain accurate information about the saturated adsorption amounts since the adsorption isotherms were performed only at the low relative pressure range of $P/P_0 < 0.029$. Hence, DR analysis was carried out for better understanding of the porous structure of the materials studied. The DR plots are given in Fig. 4. All DR plots are linear over

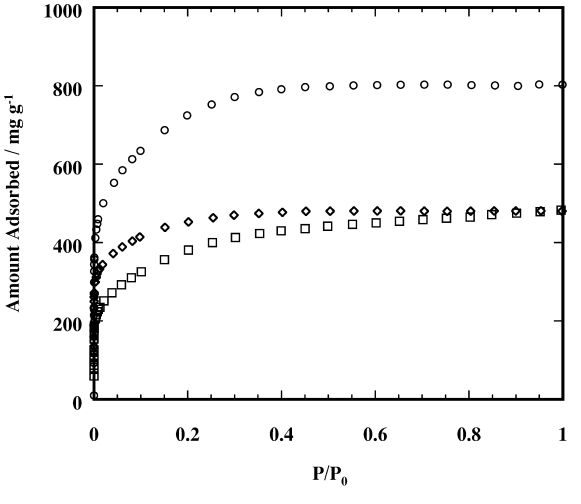

Fig. 2. N_2 adsorption isotherms on pristine and N-alloyed ACFs at 77 K: ○, ACF; □, ACF/Py1023-60; ◇, ACF/Py1273-60.

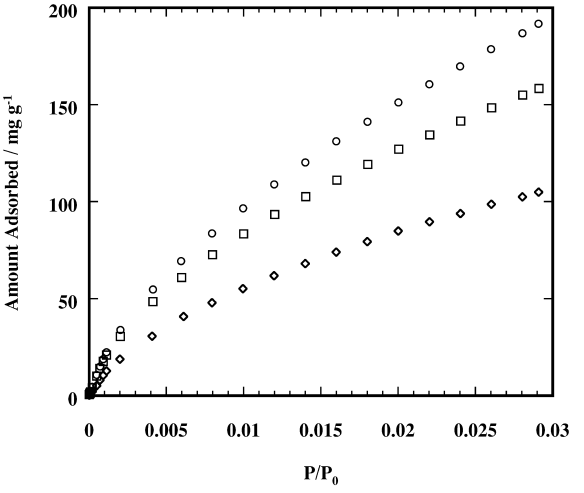

Fig. 3. Low-pressure CO_2 adsorption isotherms on pristine and N-alloyed ACFs at 273 K: ○, ACF; □, ACF/Py1023-60; ◇, ACF/Py1273-60.

the whole relative pressure range. The micropore structure parameters of the samples calculated from N_2 (77 K) and CO_2 (273 K) adsorption isotherms are summarized in Table 2. Pore volumes from the DR equation are given in Eq. (1)

$$\ln W = \ln W_0 - (A/\beta E_0)^2, \quad A = RT \ln (P_0/P). \tag{1}$$

Here, W and W_0 are the pore volume at P/P_0 and the micropore volume, respectively. A is the adsorption potential, β and E_0 are the affinity coefficient and characteristic adsorption energy. The densities used for the calculation for adsorption of N_2 (77 K) and CO_2 (273 K)

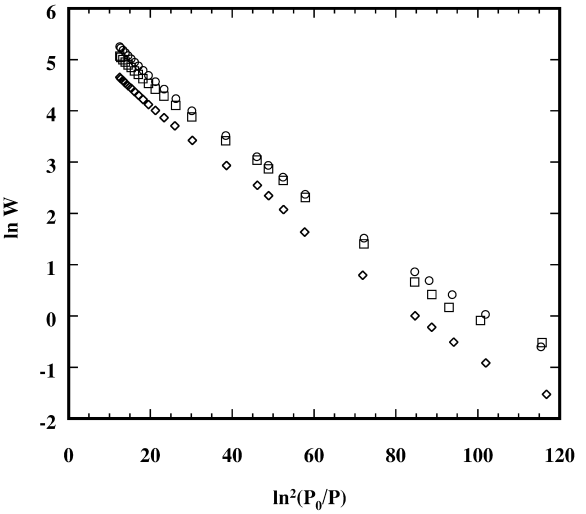

Fig. 4. DR plots of CO_2 adsorption isotherms on pristine and N-alloyed ACFs at 273 K: ○, ACF; □, ACF/Py1023-60; ◇, ACF/Py1273-60.

Table 2
Micropore structures of pristine and N-alloyed ACFs determined from N_2 and CO_2 adsorption isotherms

Sample	N_2 at 77 K[a]						CO_2 at 273 K[b]
	α_s			DR			DR
	a_α ($m^2\ g^{-1}$)	a_{ext} ($m^2\ g^{-1}$)	$W_0^{N_2-\alpha_s}$ (ml g^{-1})	$W_0^{N_2-DR}$ (ml g^{-1})	w (nm)	$q_{st,\ \phi=1/e}$ (kJ mol^{-1})	$W_0^{CO_2}$ (ml g^{-1})
ACF	2004	~0	0.99	0.75	1.09	11.7	0.51
ACF/Py1023-60	996	61	0.52	0.41	1.06	12.1	0.39
ACF/Py1273-60	1343	~0	0.58	0.48	0.89	13.0	0.26

[a] N_2 liquid density at 77 K = 0.808 g ml^{-1}.
[b] CO_2 density at 273 K = 1.023 g ml^{-1}.

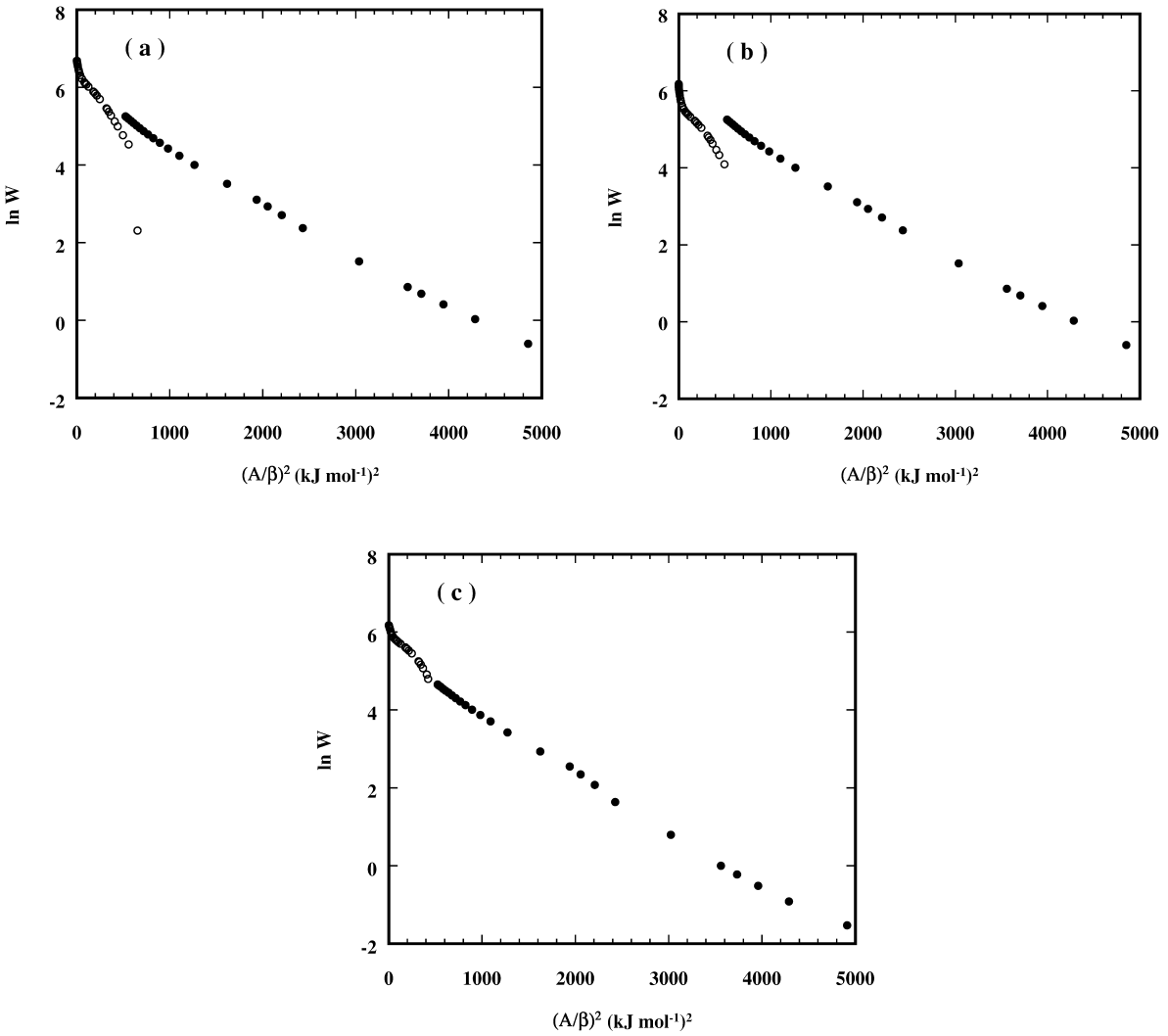

Fig. 5. Characteristic curves for pristine (a), ACF/Py1023-60 (b), and ACF/Py1273-60 (c) from N_2 (open symbol) and CO_2 (solid symbol) adsorption isotherms at 77 K and 273 K, respectively.

were 0.808 and 1.023 g ml^{-1}, respectively. The affinity coefficients of 0.33 for N_2 and 0.35 for CO_2 were used. The $W_0^{N_2-DR}$ calculated from N_2–DR plots decreases from 0.75 ml g^{-1} to 0.41–0.48 ml g^{-1} as a result of the CVD. The pyridine deposition at 1273 K narrows the pore width of ACF. The $W_0^{CO_2}$ determined from CO_2–DR plots also decreases to 0.39–0.26 ml g^{-1} from 0.51 ml g^{-1} by the pyridine-CVD. However, the $W_0^{CO_2}$ of ACF/Py1023-60 is rather large compared to that of ACF/Py1273-60. Characteristic curves were used as a more convenient way in order to compare the adsorption of N_2 and CO_2 [27–29]. Fig. 5 shows characteristic curves from N_2 and CO_2 adsorption expressed in terms of ln W and $(A/\beta)^2$. Although the overlapped abscissa range for N_2 and CO_2 is narrow, both characteristic curves can be compared. As to the characteristic curve for pristine and ACF/Py1273-60, the intercept with the perpendicular axis of N_2 data is much larger than that of CO_2 data, while ACF/Py1023-60 has an almost similar value. Pristine ACF has a large difference between $W_0^{N_2}$ and $W_0^{CO_2}$, suggesting the presence of wider microporosity [27]. This is because CO_2 molecules can be adsorbed at 273 K in narrower micropores having a deep potential wall, whereas N_2 molecules are adsorbed in all pores at 77 K. On the other hand, $W_0^{N_2}$ and $W_0^{CO_2}$ for ACF/Py1023-60 almost coincide with each other, suggesting that the CVD treatment blocks the wider pores to produce a more uniform microporous system [27]. However, the CVD treatment at higher temperature reduces the amount of the deposition and thereby the treatment cannot block effectively the wider micropores. Therefore, $W_0^{N_2}$ and $W_0^{CO_2}$ for ACF/Py1273-60 have a meaningful difference. Furthermore, βE_0 gives the isosteric heat of adsorption at fractional filling $\phi = 1/e$ with Eq. (2)

$$\beta E_0 + \Delta H_v = q_{st,\,\phi=1/e}. \quad (2)$$

Here, ΔH_v is the enthalpy of vaporization at the boiling point of the adsorbate. Nitrogen alloying increases the $q_{st,\,\phi=1/e}$ values determined from N_2 adsorption as shown in Table 2.

3.3. C_2H_5OH adsorptivity of N-alloyed ACFs

Fig. 6 shows the adsorption isotherms of C_2H_5OH on pristine and N-alloyed ACFs at 303 K. All C_2H_5OH adsorption isotherms are of type I, being analogous to the N_2 adsorption isotherms at 77 K. Hence, C_2H_5OH molecules are adsorbed by the micropore filling mechanism in a way similar to N_2 adsorption at 77 K, although the adsorption increase at the low P/P_0 range is considerably gradual. The saturated amount of C_2H_5OH adsorption of ACF/Py1023-60 is even greater than that of ACF/Py1273-60, which has greater pore volume from N_2 adsorption. However, the adsorption capacity per unit weight of N-alloyed ACFs for C_2H_5OH decreases due to reduction in the micropore volume. If we express the amount of adsorption by fractional filling, the effect of the N-alloying on C_2H_5OH adsorption will be shown clearly. Fig. 7 shows C_2H_5OH adsorption isotherms expressed in terms of fractional filling and log (P/P_0). Here the fractional filling is the ratio of the volume occupied by adsorbed C_2H_5OH to the pore volume $(W_0^{N_2-\alpha_s})$ determined by the N_2 adsorption at 77 K. ACF/Py1023-60 has the largest fractional filling of C_2H_5OH over the whole pressure range. ACF/Py1273-60 also has a larger fractional filling

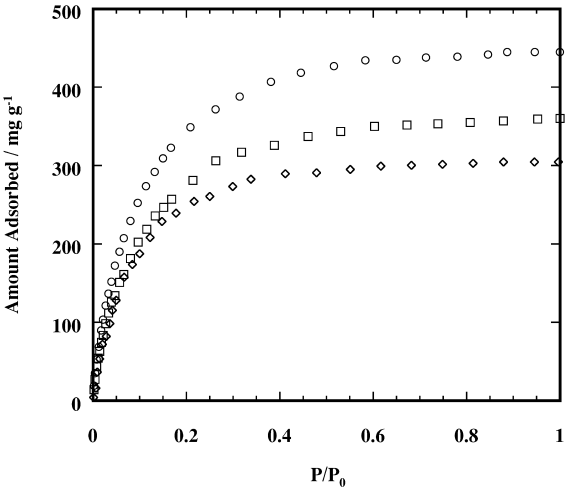

Fig. 6. C_2H_5OH adsorption isotherms on pristine and N-alloyed ACFs at 303 K: ○, ACF; □, ACF/Py1023-60; ◇, ACF/Py1273-60.

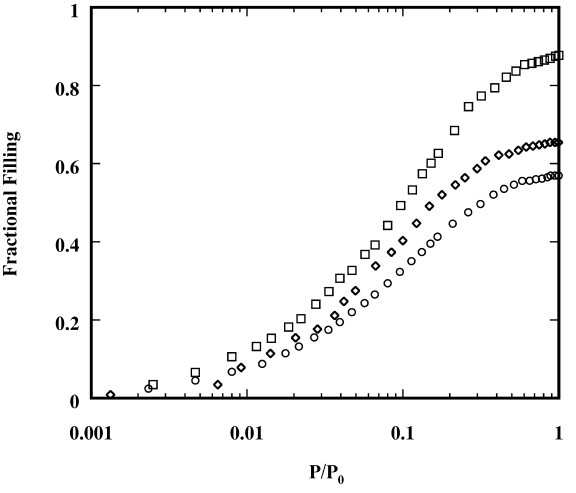

Fig. 7. Adsorption isotherms of C_2H_5OH on pristine and N-alloyed ACFs at 303 K. The amount of adsorption is expressed by fractional filling: ○, ACF; □, ACF/Py1023-60; ◇, ACF/Py1273-60.

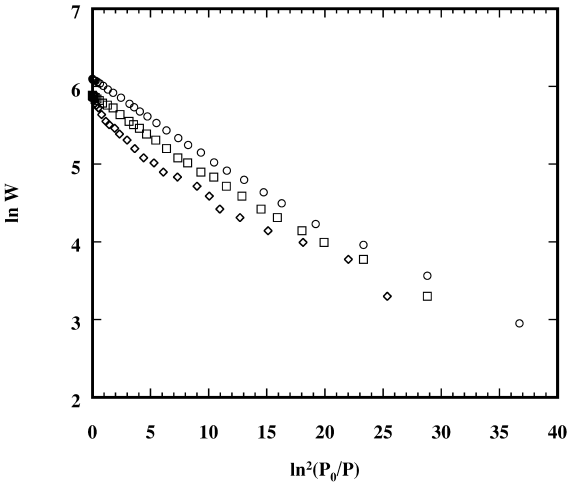

Fig. 8. DR plots of C_2H_5OH adsorption isotherms on pristine and N-alloyed ACFs at 303 K: ○, ACF; □, ACF/Py1023-60; ◇, ACF/Py1273-60.

of C_2H_5OH than pristine ACF. The nitrogen-alloying enhances remarkably the adsorptivity for C_2H_5OH molecules. These results suggest that the adsorption increase of ACF for C_2H_5OH molecules is associated with the alloyed nitrogen sites on the pore walls. Fig. 8 shows the DR plots for the C_2H_5OH adsorption isotherms. All DR plots are linear in the higher pressure range. All slopes of the DR-plots are similar. The pore volume $W_0^{C_2H_5OH}$ and $q_{st,\ \phi=1/e}$ values for C_2H_5OH–DR are shown in Table 3. Here 0.7868 g ml^{-1} of the liquid density, 0.65 of β, and 38.6 kJ mol^{-1} of ΔH_v for C_2H_5OH were used. The $q_{st,\ \phi=1/e}$ does not change due to the N-alloying. Ohkubo et al. [6] reported that C_2H_5OH molecules orientate to the micropore walls and the ordered structure depends on the pore width by use of in situ X-ray diffraction. The $W_0^{C_2H_5OH}$ values for pristine ACF and ACF/Py1273-60 are smaller than the $W_0^{N_2-DR}$ values. On the other hand, $W_0^{C_2H_5OH}$ on ACF/Py1023-60 is much larger than $W_0^{N_2-DR}$. These results clearly show that introduction of pyridinic and quaternary nitrogens in the nanographitic structure of ACF should sensitively affect the ordered structure of C_2H_5OH molecules.

3.4. H_2O adsorptivity of N-alloyed ACFs

An explicit effect by the N-alloying is observed in H_2O adsorption. Fig. 9 shows H_2O adsorption isotherms on pristine and N-alloyed ACFs at 303 K. The H_2O adsorption behavior is completely different from those of N_2 and C_2H_5OH. The adsorption isotherms of H_2O on pristine ACF are of type V, having a noticeable uptake near $P/P_0 = 0.7$ and a marked hysteresis. The steep uptake of H_2O adsorption at a medium P/P_0 is associated with cluster formation of H_2O molecules as shown in Fig. 9a. Recent in situ X-ray diffraction and in situ small angle X-ray scattering studies gave evidence for the cluster-associated filling mechanism [30–32]. The adsorption isotherm on pristine ACF has the type H2 hysteresis loop with almost vertical adsorption and desorption branches at the wide range P/P_0. H_2O adsorption isotherms on ACF/Py1023-60 and ACF/Py1273-60 are also of type V. However, ACF/Py1023-60 has the type H2 hysteresis loops with gradual adsorption and vertical desorption (Fig. 9b). ACF/Py1273-60 shows a slanting hysteresis loop of H2 (Fig. 9c). The uptake pressure of the adsorption branches of ACF/Py1023-60 and ACF/Py1273-60 shifts to a lower P/P_0, compared with that of pristine ACF. Furthermore, the desorption branch of ACF/Py1273-60 does not drop steeply even below $P/P_0 < 0.5$. Even evacuation using a rotary pump cannot remove adsorbed H_2O completely at 303 K. This irreversible adsorption should stem from the strong interaction of H_2O molecules on introduced nitrogen sites with hydrogen bonding. The irreversible amount is about 25 mg g^{-1}. This irreversible amount is 6.5% of saturated adsorption amount of H_2O. The molar ratio of irreversible H_2O molecules to the alloyed surface nitrogen sites obtained from elemental analysis is about 1.24. Accordingly it is probable that a H_2O molecule is adsorbed on a nitrogen site by the hydrogen bond. H_2O adsorption isotherms on ACF/

Table 3
Micropore volume $W_0^{C_2H_5OH}$ and isosteric heat of adsorption $q_{st,\ \phi=1/e}$ (C_2H_5OH) from C_2H_5OH adsorption isotherms (303 K), saturated adsorption amount of H_2O (V^{H_2O}) from H_2O adsorption isotherms (303 K), and saturated adsorption amount of N_2 (V^{N_2}) from N_2 adsorption isotherms (77 K)

Sample	$W_0^{C_2H_5OH}$ (ml g^{-1})	$q_{st,\ \phi=1/e}$ (C_2H_5OH) (kJ mol^{-1})	V^{H_2O} (ml g^{-1})	V^{N_2} (ml g^{-1})
ACF	0.57	46.5	0.57	0.64
ACF/Py1023-60	0.47	46.2	0.47	0.38
ACF/Py1273-60	0.39	46.3	0.41	0.39

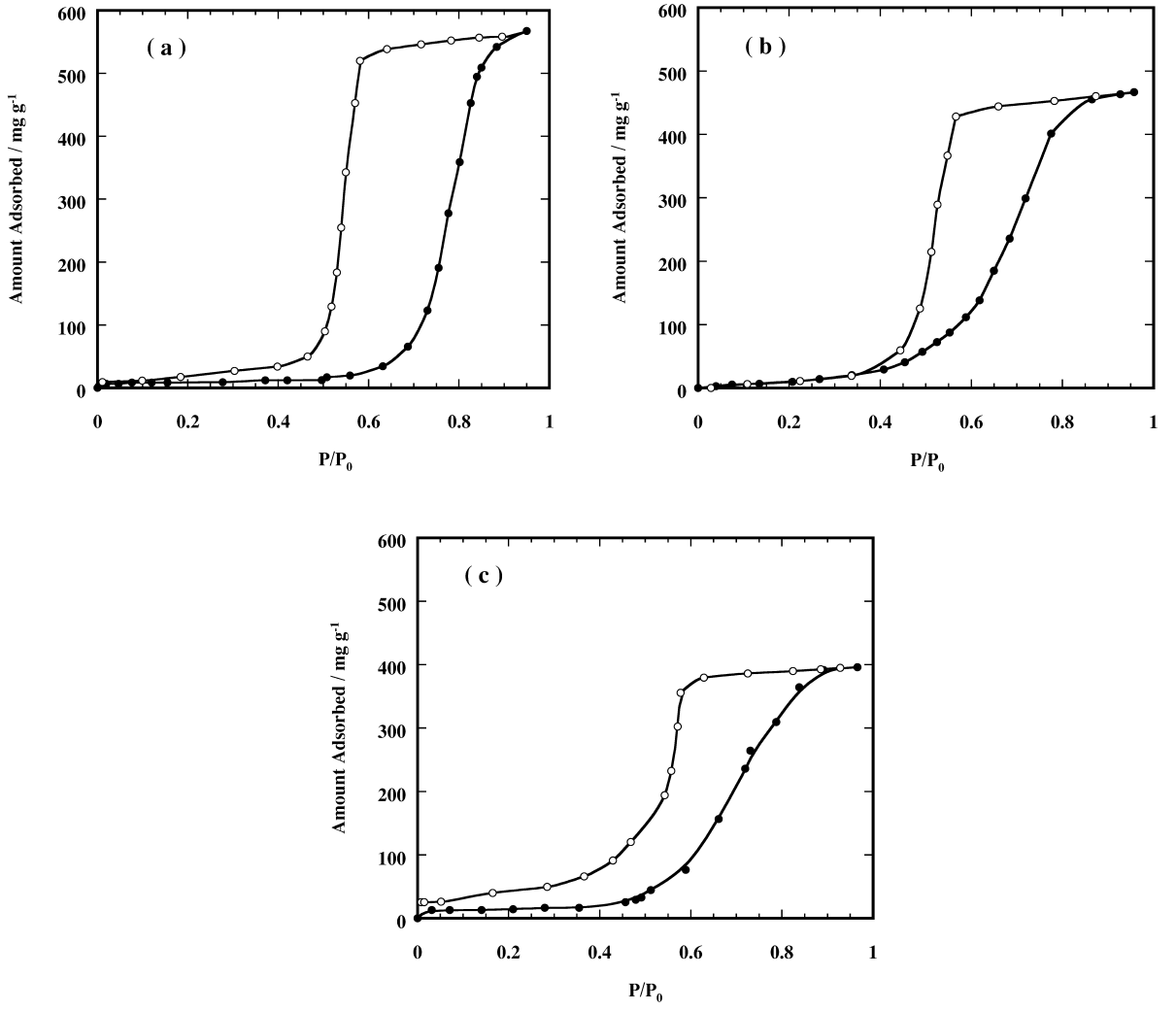

Fig. 9. H_2O adsorption isotherms of pristine (a), ACF/Py1023-60 (b), and ACF/Py1273-60 (c) at 303 K. Solid and open symbols indicate adsorption and desorption branches, respectively.

Py1023-60 and ACF/Py1273-60 have a gradual adsorption uptake even from $P/P_0 < 0.1$. The H_2O adsorption at the low P/P_0 range comes from the presence of pyridinic sites in ultramicropores.

The saturated amount of H_2O adsorption, V^{H_2O}, determined by the extrapolation of the isotherm to $P/P_0 = 1$ is summarized in Table 3. $W_0^{N_2-\alpha_s}$ values of pristine ACF and ACF/Py1273-60 are much greater than V^{H_2O} ones. On the other hand, $W_0^{N_2-\alpha_s}$ and V^{H_2O} values of ACF/Py1023-60 are almost similar. The ratios of the V^{H_2O} to $W_0^{N_2-\alpha_s}$ are 0.58, 0.90, and 0.70 for pristine ACF, ACF/Py1023-60, and ACF/Py1273-60, respectively. These data indicate precisely that pyridinic sites are more effective for inducing H_2O adsorption than quaternary nitrogen sites. Although ACF/Py1273-60 has also charged nitrogen sites on the pore-walls, H_2O molecules form a more ordered structure having a smaller density in the narrow micropores ($w = 0.89$ nm) of ACF/Py1273-60. Thus, the amount of nitrogen, state of doped nitrogen, and the pore width considerably affect the H_2O adsorption of ACF.

Acknowledgements

This work was funded by Grant in Aid for Scientific Research on Priority Areas No. 288 ‘Carbon Alloys’ from the Japanese Government.

References

[1] Kaneko K. Stud Surf Sci Catal 1993;99:573–98.
[2] Kaneko K. J Membr Sci 1994;96:59–89.
[3] Kaneko K. Stud Surf Sci Catal 1998;120:635–58.
[4] Iiyama T, Nishikawa K, Otowa T, Suzuki T, Kaneko K. In: McEnaney B, May TJ, Rouquerol J, Rodriguez-Reinoso F, Sing KSW, Unger KK, editors, Characterisation of porous solids, vol. IV, London: Royal Society of Chemistry, 1998, pp. 41–8.
[5] Wang ZM, Kaneko K. J Phys Chem B 1998;102:2863–8.
[6] Ohkubo T, Iiyama T, Nishikawa K, Suzuki T, Kaneko K. J Phys Chem B 1999;103:1859–63.
[7] Marquez-Alvarez C, Rodriguez-Ramos I, Guerrero-Ruiz A. Carbon 1996;34:1509–14.
[8] Kaneko K, Kobayashi A, Suzuki T, Ozeki S, Kakei K, Kosugi N et al. J Chem Soc Faraday Trans 1 1988;84:1795–805.
[9] Kaneko K, Kosugi N, Kuroda H. J Chem Soc Faraday Trans 1 1989;85:869–81.
[10] Kaneko K. Colloids Surf 1989;37:115–24.
[11] Nishi Y, Suzuki T, Kaneko K. J Phys Chem B 1997;101:1938–9.
[12] Nishi Y, Suzuki T, Kaneko K. Carbon 1998;36:1870–1.
[13] El-Merraoui M, Tamai H, Yasuda H, Kanata T, Mondori J, Kadai K et al. Carbon 1998;36:1769–74.
[14] Mangun CL, Benak KR, Daley MA, Economy J. Chem Mater 1999;11:3476–83.
[15] Lee WH, Reucroft PJ. Carbon 1999;37:7–14.
[16] Rodriguez-Reinoso F, Molina-Sabio M, Munecas MA. J Phys Chem 1992;96:2707–13.
[17] Kaneko Y, Ohbu K, Uekawa N, Fujie K, Kaneko K. Langmuir 1995;11:708–10.
[18] Yang CM, El-Merraoui M, Kaneko K. Langmuir, submitted.
[19] Kawabuchi Y, Sotowa C, Kishino M, Kawano S, Whitehurst DD, Mochida I. Langmuir 1997;13:2314–7.
[20] Kawabuchi Y, Sotowa C, Kishino M, Kawano S, Whitehurst DD, Mochida I. Chem Lett 1996;:941–2.
[21] Sotowa C, Kawabuchi Y, Mochida I. Chem Lett 1996;:967–8.
[22] Briggs D, Seah MP. Practical surface analysis by Auger and X-ray photoelectron spectroscopy, Wiley: Chichester, 1995.
[23] Hughes AE, Sexton BA. J Electron Spectrosc Relat Phenom 1988;46:31–42.
[24] Darmstadt H, Roy C, Kaliaguine S. Carbon 1994;32:1399–406.
[25] Gardner SD, Singamsetty CSK, Booth GL, He GR. Carbon 1995;33:587–95.
[26] Yue ZR, Jiang W, Wang L, Gardner SD, Pittman Jr. CU. Carbon 1999;37:1785–96.
[27] Garrido J, Linares-Solano A, Martin-Martinez JM, Molina-Sabio M, Rodriguez-Reinoso F, Torregrosa R. Langmuir 1987;3:76–81.
[28] Cazorla-Amoros D, Alcaniz-Monge J, Linares-Solano A. Langmuir 1996;12:2820–4.
[29] Molina-Sabio M, Munecas MA, Rodriguez-Reinoso F, Mcenaney B. Carbon 1995;33:1777–82.
[30] Kaneko K, Hanzawa Y, Iiyama T, Kanda T, Suzuki T. Adsorption 1999;5:7–13.
[31] Iiyama T, Ruike M, Kaneko K. Chem Phys Lett 2000;, In press.
[32] Iiyama T, Nishikwa K, Otowa T, Kaneko K. J Phys Chem 1995;99:10075–6.